Nonlinear Dyn (2019) 96:2157–2177
https://doi.org/10.1007/s11071-019-04915-9

ORIGINAL PAPER

Deep neural network for unsteady aerodynamic and aeroelastic modeling across multiple Mach numbers

Kai Li · Jiaqing Kou · Weiwei Zhang

Received: 1 September 2018 / Accepted: 21 March 2019 / Published online: 3 April 2019

Abstract Aerodynamic reduced-order model (ROM) is a useful tool to predict nonlinear unsteady aerodynamics with reasonable accuracy and very low computational cost. The efficacy of this method has been validated by many recent studies. However, the generalization capability of aerodynamic ROMs with respect to different flow conditions and different aeroelastic parameters should be further improved. In order to enhance the predicting capability of ROM for varying operating conditions, this paper presents an unsteady aerodynamic model based on long short-term memory (LSTM) network from deep learning theory for large training dataset and sampling space. This type of network has attractive potential in modeling temporal sequence data, which is well suited for capturing the time-delayed effects of unsteady aerodynamics. Different from traditional reduced-order models, the current model based on LSTM network does not require the selection of delay orders. The performance of the proposed model is evaluated by a NACA 64A010 airfoil pitching and plunging in the transonic flow across multiple Mach numbers. It is demonstrated that the model can accurately capture the dynamic characteristics of aerodynamic and aeroelastic systems for varying flow and structural parameters.

K. Li · J. Kou (✉) · W. Zhang
School of Aeronautics, Northwestern Polytechnical University, Xi'an 710072, China
e-mail: koujiaqing93@163.com

Keywords Unsteady aerodynamic · Transonic flow · Long short-term memory network · Limit-cycle oscillation · Reduced-order model

1 Introduction

Currently, the prediction of unsteady flow dynamic is primarily achieved by high-fidelity computational fluid dynamics (CFD) method. However, the high computational cost of the CFD technique makes it very inefficient in some engineering applications, like system control [1–3] and optimization design [4], multi-field coupling [5–7] and so on. To maintain a balance between accuracy and computational efficiency for aerodynamic simulation, researchers have developed a group of unsteady flow reduced-order models (ROMs) [8–10] based on CFD method. According to the difference of mathematical method, model construction and data source, these models can be broadly divided into two types: One is to extract the main features of flow by some projection-based methods and the other includes system identification-based methods. Feature extraction methods determine the low-order subspaces through projecting the high-dimensional flow data onto several low-order bases, thus decreasing the complexity and computational cost of system [11,12]. However, system identification-based methods, using input–output data measured from a system of interest, describe the system from a black-box framework with a brief mathematical expression.

Because system identification-based ROMs are constructed by black-box methods, the training process of these models is independent to the governing equations of the systems. With a simple input–output representation, these models improve the efficacy of numerical simulation dramatically. There have been some investigations on structural dynamics field, using system identification methods [13,14]. Moreover, these approaches are well welcomed in dealing with problems concerning dynamic responses, like flutter and limit-cycle oscillations (LCOs) of aeroelastic systems. Many system identification methods, including the autoregressive with exogenous input (ARX) model [15], the radial basis function (RBF) neural network [16] and Kriging [17], have been successfully used in predicting aerodynamic loads [18].

A typical application of unsteady aerodynamic ROMs is aeroelasticity. Aeroelasticity focuses on the interaction between an unsteady flowfield and a flexible structure. Nonlinear effects of the aeroelastic system come from both aerodynamic forces and structural motion. Shock waves, viscous effects and separated flows in aerodynamic flows result in the aerodynamic nonlinearities, while structural nonlinearities are always induced by control surface freeplay and geometric structural nonlinearities. When any of nonlinear characteristic exists, LCOs can be induced. In the current study, nonlinear behavior induced by unsteady aerodynamics is focused, which relies on the construction of accurate aerodynamic ROMs for fast simulation. The ROMs should cover both linear and nonlinear aerodynamic features, in order to predict both flutter and LCO responses accurately. Among many existing ROMs, neural network, which is flexible with fault-tolerant ability and approximates any functions to high accuracy, is gaining more and more concentration [19,20]. For example, Zhang et al. [16] and Mannarino et al. [21] predicted the LCO behaviors induced by nonlinear aerodynamic by means of recursive and recurrent neural networks (RNNs). However, due to the shallow neural network architecture, these models have difficulty dealing with problems with large samples, thus limited at the modeling of single Mach number.

Although system identification-based ROMs have been validated to be effective in reproducing aerodynamic loads with a constant operating condition, ROMs across multiple operating conditions are of great interest. This is because in real applications, the condition of interest may change, but the model is also required to be valid. Currently, an interpolation method based on the Grassmann manifold and its tangent space at a point that is applicable to aeroelastic system was proposed by Amsallem and Farhat [22]. However, the results for these adaptations can be worse as Mach numbers becoming far from each other. Skujins and Cesnik [23] developed a single ROM across multiple Mach numbers by combining linear convolution with a nonlinear correction factor. Nevertheless, there exists a distinct phase shift at higher oscillation frequencies. A neurofuzzy-model-based unsteady aerodynamic ROM is proposed by Winter and Breitsamber [24]. A three-layered neural network is trained by local linear model tree algorithm to analyze the flutter boundary of an AGARD 445.6 wing from subsonic to hypersonic flows in this ROM. However, this ROM does not concern LCO behaviors. Later, a ROM based on interpolation method was presented for an elastic wing with two control surfaces by Liu et al. [25]. The application of this approach demonstrates the efficient and acceptable prediction for Mach number 0.85–0.90. In summary, although there are some models with multiple Mach numbers, model accuracy [26] and predictive capability [27] for nonlinear aeroelastic phenomenon still need to be improved.

To construct aerodynamic ROMs for multiple operating points, two problems exist. The first is that the dynamic behaviors changing with the parameter are very complicated, since both the nonlinearity for one operating point and across the modeling operating conditions should be modeled accurately. The second problem is that to have an accurate parameter-varying model, a large number of data points are needed for modeling training. Therefore, the ROMs should capture extremely complicated dynamics from a large dataset. To solve such problems, deep neural networks, which are able to model complex nonlinearity and large dataset, are needed. Currently, nearly all aerodynamic models based on neural networks are shallow neural networks, which only achieved good results in the simulation of aerodynamic modeling with small samples and constant flow condition [28].

Recently, with the development of algorithms and computational capability, deep learning (DL) has attracted widespread attention, which outperforms other machine learning methods in numerous important applications [29], like image processing, video and speech recognition, genetics and disease diagnosis [30–32], nonlinear system identification [33,34]. More

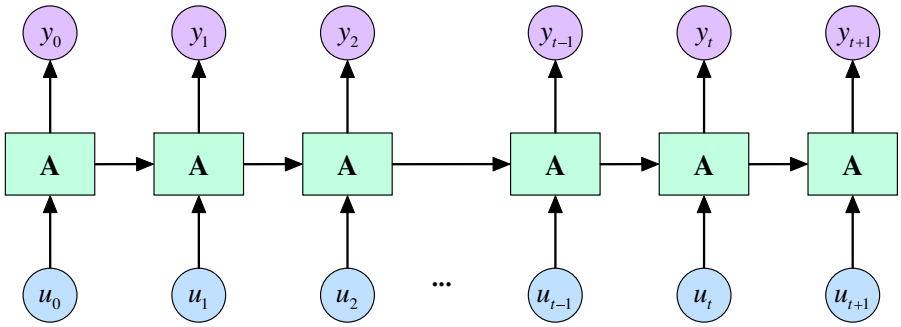

Fig. 1 LSTM architectures

recently, there have been some applications of DL in fluid dynamics, such as turbulence modeling. For example, Ling et al. are the first to apply a true deep neural networks (DNNs) architecture to Reynolds averaged Navier–Stokes turbulence models, using high-fidelity simulation data to train DNN in order to enhance prediction accuracy [35]. As a typical DNN, long short-term memory network (LSTM) is well suited to classify, process and predict time series with time lags of unknown size and duration between important events. Recently, it has outperformed traditional neural networks in speech recognition and video processing and has become a very popular method in many major IT companies [36,37]. LSTM network is also utilized in traffic flow prediction by Zhao et al. [38] and Fu et al. [39], and a comparison with other representative models validates that LSTM network can achieve a better performance. Wang et al. [40] developed a ROM based on LSTM network and proper orthogonal decomposition (POD) method, studying two numerical problems, flow past a cylinder and a wind-driven ocean gyre. Moreover, it is demonstrated that this ROM is capable of capturing complex characteristics of flow dynamic and predicting the evolution of flow. Besides, Mohan and Gaitonde did the similar research [41]. Those works focused mainly on the evolution of flow, rather than the application of aeroelastic problems. As neural networks with deep architecture, LSTM network can process large data and learn more hidden information from nonlinear systems in order to predict [42] by multiple levels of representation. Therefore, long short-term memory and nonlinear mapping features of LSTM network provide a very good thought for establishing nonlinear and unsteady aerodynamic models.

In this work, an unsteady aerodynamic ROM with varying Mach numbers based on LSTM network is proposed. Unlike most of works in the previous study, the proposed model is capable of treating a large number of training samples, with the capability of predicting aerodynamic loads in a wide range of Mach numbers. The performance of the proposed model is evaluated by predicting the aerodynamic and aeroelastic responses of a NACA 64A010 airfoil in the transonic flow. It is proved that the results from the proposed model agree with those of the CFD solver very well.

2 Methods

2.1 LSTM

LSTM network was presented by Sepp Hochreiter and Jurgen Schmidhuber in 1997 [43], which is a typical deep learning method for time sequence data. It is essentially a system identification-based method and has great potential for taking account for unsteady time-delayed effects. LSTM network is a special variant of RNN, which overcomes stability bottlenecks encountered in traditional RNNs, like the vanishing gradient [44]. Different from traditional unsteady aerodynamic modeling based on RNN [21], the user does not need to assign delay orders for LSTM network, since the time-delayed effects are considered by the network itself. This dramatically reduces the difficulty of model training. Thus, the proposed approach is a potential tool for unsteady aerodynamic modeling.

The architecture of LSTM network used in this work is shown in Fig. 1. We consider the inputs and outputs of the hidden units (i.e., units that are not in the input or output layer) at different discrete time steps, as if they were the inputs and outputs of different neurons in a deep multilayer network, in which all the layers share the same weights. Then, it becomes clear how we can utilize backpropagation, which is an algorithm to indicate how a machine should change its internal param-

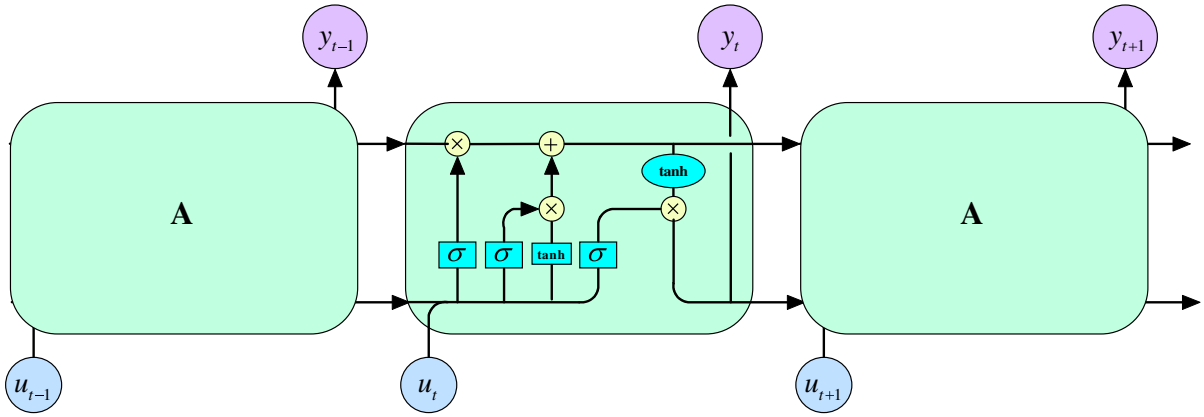

Fig. 2 Architecture of LSTM cell with various gates

eters, to train LSTM network [42]. In other words, the outputs of a discrete time step depend on the outputs and inputs of the previous time step and the inputs of this time step. Moreover, the memory block of LSTM learns the underlying relationship of input–output data at a time step. The structure of LSTM cell is illustrated in Fig. 2. In addition, the LSTM cell contains three gates: the input gate, output gate and the forget gate. The equations to compute these gates and states are as follows:

$$\begin{aligned} i_t &= \sigma(W_i \cdot [y_{t-1}, u_t] + b_i) \\ \tilde{C}_t &= \tanh(W_C \cdot [y_{t-1}, u_t] + b_C) \\ f_t &= \sigma(W_f \cdot [y_{t-1}, u_t] + b_f) \\ C_t &= f_t * C_{t-1} + i_t * \tilde{C}_t \\ o_t &= \sigma(W_o \cdot [y_{t-1}, u_t] + b_o) \\ y_t &= o_t * \tanh(C_t) \end{aligned} \tag{1}$$

The input, output and forget gates are represented by i, o and f, respectively. C denotes the cell state and is a linear equation as shown in (1), thus changing slowly in the time dimension. The cell input and output are given by u and y, respectively, where y also means the short-term memory state and is a multiplicative equation as illustrated in (1), thus changing dramatically. W denotes the weight matrices, and σ and tanh are sigmoid and tanh activation functions, respectively, as shown in (2). In this paper, the Keras libraries in python are used to train and simulate the LSTM network [45].

$$\begin{aligned} \sigma(x) &= \frac{1}{1+e^{-x}} \\ \tanh(x) &= \frac{e^x - e^{-x}}{e^x + e^{-x}} \end{aligned} \tag{2}$$

2.2 Unsteady aerodynamic modeling

In this work, the input variables of unsteady aerodynamic ROM are Mach number, transonic NACA64A010 airfoil plunging displacement and pitching angle. The output variables are the lift and pitch moment coefficients. The purpose of unsteady aerodynamic modeling through LSTM neural network is to identify a nonlinear mathematical relationship between system input and output: i.e., $y_t = f(u_t, y_{t-1}, C_{t-1})$, where u and $y$are input and output, respectively, and t is the current time instant. Different from typical aerodynamic models, time delay effect is reflected in function f, rather than expressed as a nonlinear autoregressive with exogenous input framework [46].

There are three sets of data: training samples, validation samples and test samples [47]. Training samples are used for determining the unknown model parameters. Validation case, which is totally different from the training case, is used to evaluate the model performance during the training process. Note that this case is not used for training, but is able to determine the optimal model, as can be seen in the early-stopping method [48]. And the test case is used only when the model is needed for practical use. The main steps to construct the proposed ROM by LSTM network are as follows:

(a) Collect the training samples under some Mach numbers from CFD simulations.
(b) Calculate the validation samples with small amplitude under the same Mach numbers for evaluating the generalization capability of the proposed model.

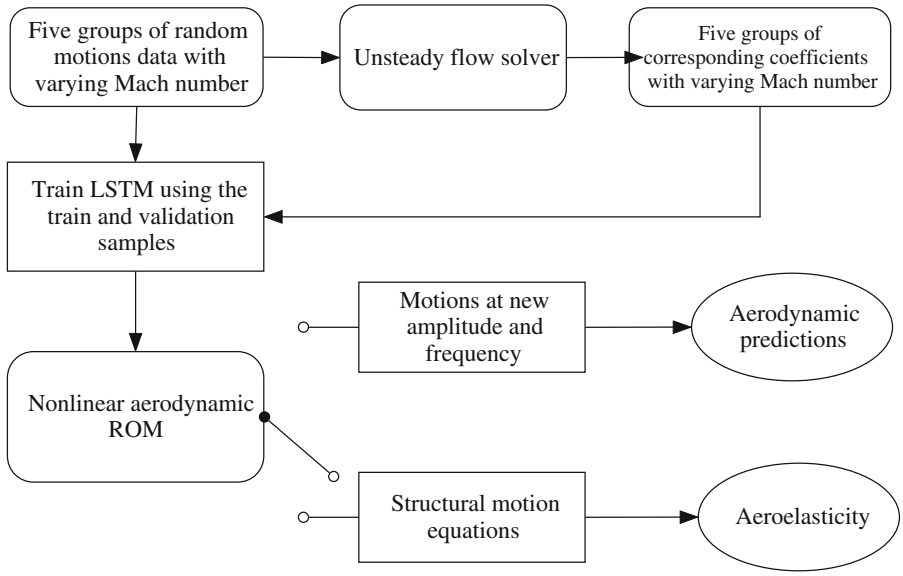

Fig. 3 Flowchart of applications based on ROM

(c) Train LSTM model using the training and validation samples.
(d) Substitute LSTM network for CFD simulations after training for further research and analysis (test case).

The flowchart of applying the proposed approaches is shown in Fig. 3. In this paper, two types of applications are considered. It should be noted that the aerodynamic model is the same, but the only difference is that for aeroelasticity, the model is coupled with the structural motion equation, while for aerodynamic simulation, no coupling is considered. These applications are summarized as follows:

1. Given the structural motions, the unsteady and nonlinear aerodynamic loads are predicted by this ROM. A prescribed kind of motion is imposed as the input signal, and the corresponding aerodynamic coefficients are predicted.
2. Coupling the structural equations of motion and unsteady aerodynamic ROM, the responses of aeroelastic system are determined by time marching the governing equations. Specially, at each time step, the aerodynamic load is predicted and then the structural equation is calculated according to current aerodynamic load, and then it moves to the next time step. The structure and aerodynamic system are loosely coupled for aeroelastic simulation.

3 Time-marching method of the aeroelastic systems

3.1 Flow solver

An unsteady flow solver based on both Euler and Reynolds-average Navier–Stokes equations is adopted in the current investigation. For the current study, the Euler solver is used. A cell-centered finite-volume formation using a center-differencing scheme is applied for spatial discretization, while the governing equations are non-dimensionalized by the mean aerodynamic chord c, speed of sound a_∞ and freestream temperature T_∞. Further details of numerical methods can be found in [49]. A dynamically deforming mesh algorithm based on RBF interpolation [50] is used in this work. Our CFD solver has been tested in some cases like flutter or buffet phenomenon [51,52].

3.2 Structural equations of motion

A typical two-dimensional aeroelastic model with two degrees of freedom in plunge and pitch is shown in Fig. 4. The following equation is the structure equation of motion:

$$\begin{bmatrix} 1 & x_\alpha \\ x_\alpha & r_\alpha^2 \end{bmatrix} \begin{Bmatrix} \ddot{h}/b \\ \ddot{\alpha} \end{Bmatrix} + \begin{bmatrix} (\omega_h/\omega_\alpha)^2 & 0 \\ 0 & r_\alpha^2 \end{bmatrix} \begin{Bmatrix} h/b \\ \alpha \end{Bmatrix} = \frac{1}{\pi}(V^*)^2 \begin{Bmatrix} -C_\mathrm{l} \\ 2C_\mathrm{m} \end{Bmatrix} \tag{3}$$

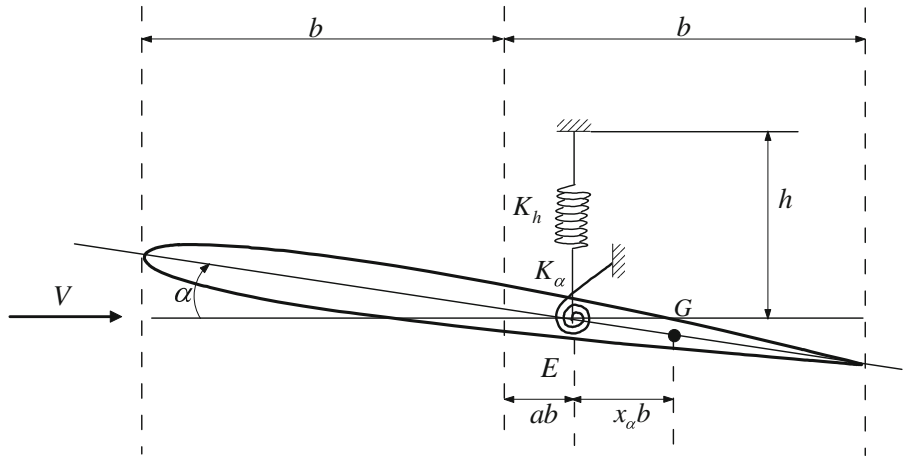

Fig. 4 Aeroelastic model with two degrees of freedom

where h and α are the airfoil plunging displacement and pitching angle, respectively. C_l and C_M are the lift and pitch moment coefficients, respectively. r_a is the gyration radius of the airfoil around the elastic axis. x_a is the airfoil static unbalance (dimensionless distance between the center of gravity and the hinge axis). ω_h and ω_α are the uncoupled natural frequencies of the plunge and pitch, respectively. V^* is the reduced velocity, which is defined as follows:

$$\begin{aligned} V^* &= V/(\omega_\alpha \cdot b \cdot \sqrt{\mu}) \\ \mu &= \frac{m_\alpha}{\pi \rho_\infty b^2} \end{aligned} \tag{4}$$

where b, μ and V are the half-chord length, mass ratio and freestream velocity, respectively. (3) can be written in matrix form as (5), where $\boldsymbol{M}$, $\boldsymbol{K}$, $\boldsymbol{Q}$, $\boldsymbol{\xi}$ are the generalized mass, stiffness matrices, generalized force vector and structural coordinate vector, respectively.

$$\boldsymbol{M}\ddot{\boldsymbol{\xi}} + \boldsymbol{K}\boldsymbol{\xi} = \boldsymbol{Q} \tag{5}$$

After transforming (5) into a state-space representation, the fourth-order accuracy hybrid linear multistep method [53] is utilized to solve the aeroelastic equation in the time domain, where the predictor–corrector method is used. In the predictor procedure, both structural and aerodynamic parts are expanded in explicit scheme; however, in the corrector step, only the aerodynamic part is expanded in the explicit scheme, whereas the structural part is expanded in the implicit scheme.

Using the above-mentioned numerical method, the structural response at a given Mach number and V^* can be solved in the time domain, and the aeroelastic characteristics can be obtained. The aerodynamic time step is non-dimensionalized as follows:

$$DT = \mathrm{d}t/(2 \cdot b/a_\infty) \tag{6}$$

where dt is the physical time step.

4 Results and discussion

In this paper, unsteady aerodynamics of a NACA 64A010 airfoil with two degrees of freedom across multiple Mach numbers in the transonic flow is identified. Both unsteady aerodynamic and nonlinear aeroelastic simulations are performed. Firstly, by using the unsteady aerodynamic ROM across multiple Mach numbers, aerodynamic loads under harmonic motions at different Mach numbers, amplitudes and frequencies are predicted in the time and frequency domain, respectively. Results are compared with those from CFD. Next, the LCO trends under a range of Mach numbers and at different structural parameters are considered, in order to evaluate that the proposed approach can accurately capture the dynamic characteristics of aerodynamic and aeroelastic response for varying flow and structural parameters.

In this paper, the unit number of LSTM network is 32. The number of hidden layers is a hyper-parameter for LSTM, which is selected as 1 in the current study. Increasing the number of hidden layers leads to a decline in the computational efficiency. However, the works of Graves [54] and Pascanu [55] have demonstrated that shallow LSTM network can still achieve

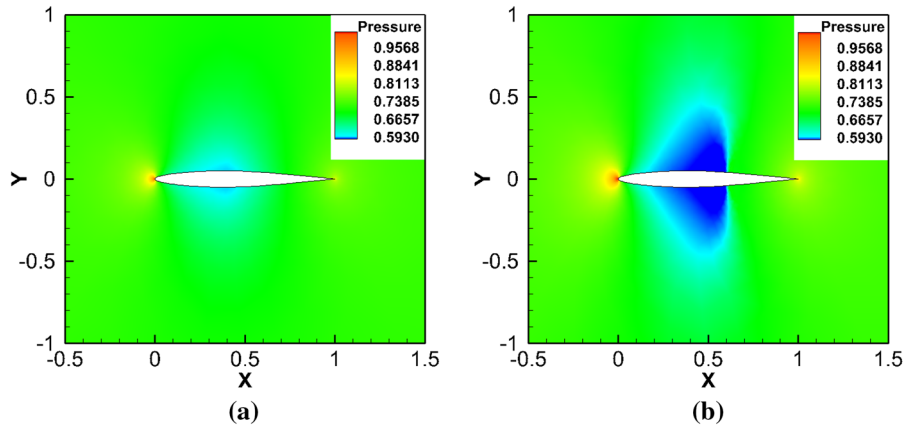

Fig. 5 Steady pressure distributions of two typical flow conditions. **a** $Ma = 0.74$. **b** $Ma = 0.82$

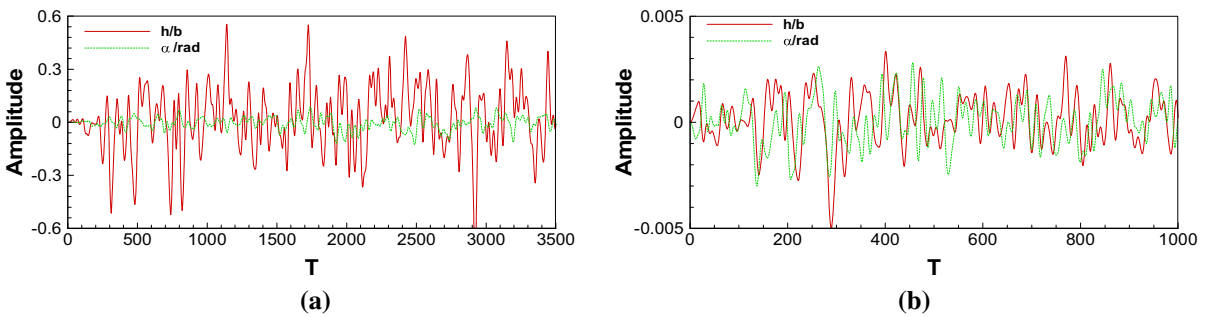

Fig. 6 **a** Training inputs with 3500 time steps. **b** Validation inputs with 1000 time steps

good performance in modeling. Unlike other shallow neural networks, there are special memory cells and deep multilayers in the time dimension for LSTM network. In training the model for backpropagation through time (BPTT), Adam optimizer with adaptive learning rates is utilized to minimize training error and meanwhile avoid local minimal point [39,56].

4.1 Training and validation case

Five transonic Mach numbers [0.74, 0.76, 0.78, 0.80, 0.82] are selected as the variable space of training and validation samples. Since the investigated flow regime is within the scope of transonic flow, it is still a difficult work for accurate simulations in the Mach number range of 0.08. This is further shown in Fig. 5, where the steady flow contours of $Ma = 0.74$ and $Ma = 0.82$ are given. It can be observed that it varied drastically for the flow from the minimal to the maximal Mach numbers, which also means that the selected Mach number range is large enough for multiple nonlinear characteristics. More details about the comparison of dynamic behaviors across the training Mach number range are given in [26].

To cover wide ranges of amplitude and frequency, the excitation signals used for training and validating ROM are designed as two filtered white Gaussian noise (FWGN) signals, which include 3500 and 1000 time steps at all Mach numbers, respectively, as shown in Fig. 6. In order to capture both high- and low-frequency characteristics, the aerodynamic time step DT is set to 0.6 and 0.4 for ROM and CFD simulations, respectively. The proposed ROM is a MIMO system, where the input and output vectors are defined as:

$$\begin{aligned} u_t &= [\,(h/b)_t \quad \alpha_t \quad Ma\,] \\ y_t &= [\,(C_\mathrm{l})_t \quad (C_\mathrm{m})_t\,] \end{aligned} \tag{7}$$

The dynamic characteristics across the selected Mach number range are compared in Fig. 7. As seen in this figure, for the same type of motion, a large discrepancy in the aerodynamic response across the training Mach number range is observed.

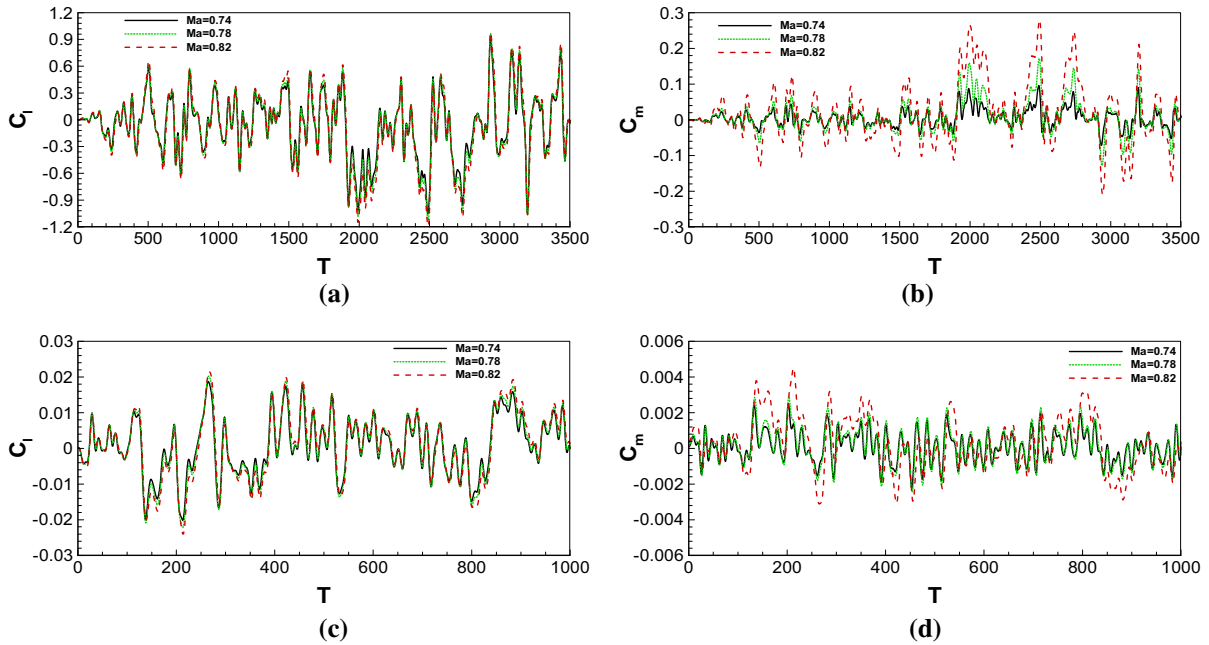

Fig. 7 Aerodynamic loads computed from CFD simulations at three Mach numbers. **a** Lift coefficient of training case. **b** Moment coefficients of training case. **c** Lift coefficient of validation case. **d** Moment coefficients of validation case

Since the gradient decreasing method is used for model training, to analyze the uncertainty of LSTM network, ten different LSTM models are obtained by training the model ten times and are compared together. A random motion with two degrees of freedom at $Ma = 0.77$ is used to test the model performance. Then, the results obtained from those LSTM models and CFD simulations are compared. Figure 8 shows comparison between CFD simulations and the error band from results of those models. As seen in this figure, the model output varies little with different training initial conditions. This is further validated by comparing the relative error of each model in predicting the random motions at four different Mach numbers, which is illustrated in Fig. 9. Note that the selected Mach numbers for model evaluation are different from those for model training. The relative error used for model evaluation is defined as:

$$RE = \frac{\|\boldsymbol{y}_{\mathrm{ROM}} - \boldsymbol{y}_{\mathrm{CFD}}\|_F}{\|\boldsymbol{y}_{\mathrm{CFD}}\|_F} \times 100\% \tag{8}$$

where the result of ROM is represented by $\boldsymbol{y}_{\mathrm{ROM}}$, while $\boldsymbol{y}_{\mathrm{CFD}}$ denotes the result obtained from CFD simulations. From Figs. 8 and 9, it is demonstrated that a small

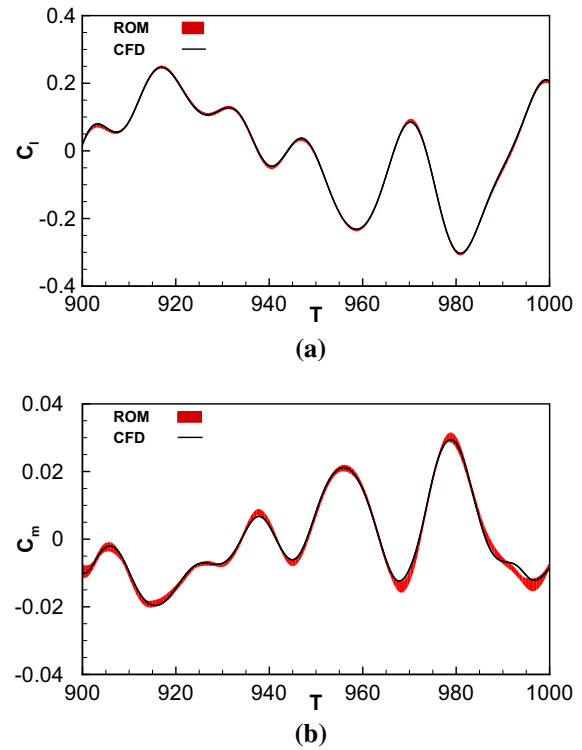

Fig. 8 Comparison of aerodynamic loads for a random motion at $Ma = 0.77$ between CFD simulations and the error band from results of ten models. **a** Lift coefficient. **b** Moment coefficients

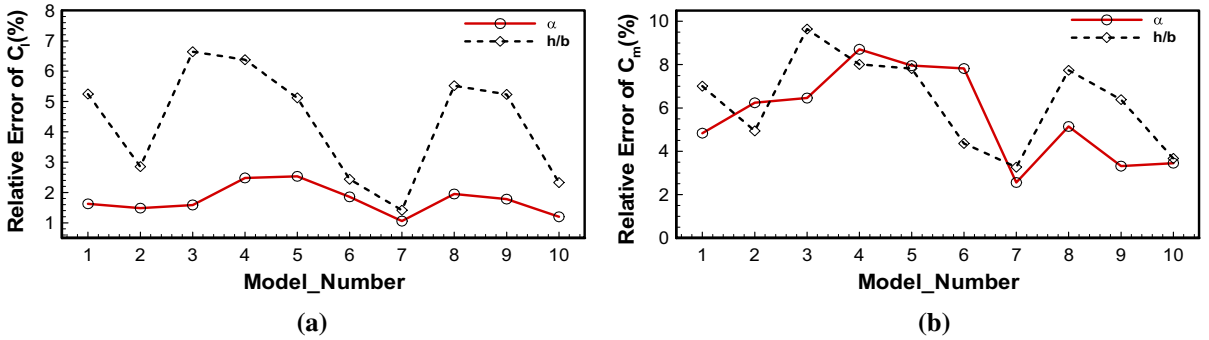

Fig. 9 Mean relative error of aerodynamic loads for random motions at $Ma = 0.75, 0.77, 0.79$ and 0.81. **a** Lift coefficient. **b** Moment coefficients

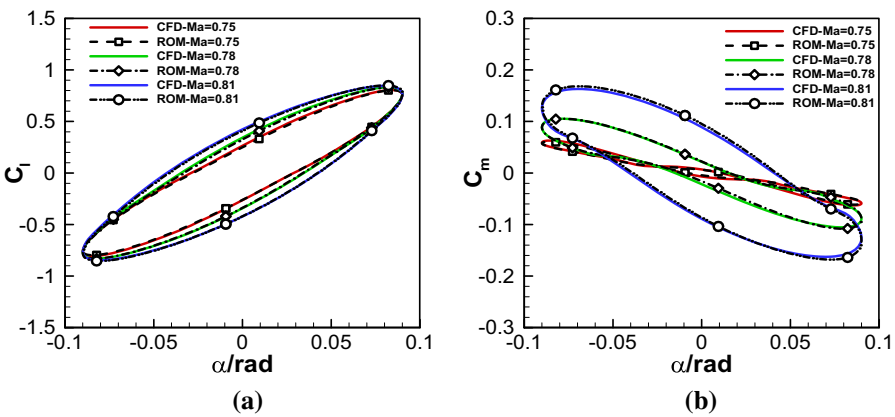

Fig. 10 Predictions of harmonic motions with pitching amplitude 0.09 and 120 steps in a period under different Mach number. **a** Lift coefficient. **b** Moment coefficients

discrepancy among those models is observed, indicating that the proposed model is robust to initial training conditions.

4.2 Unsteady aerodynamics simulations

In order to estimate the overall model performance, No. 1 model in Fig. 9 is chosen for the following study because of its average performance among these models. The test cases used to evaluate the performance of this ROM are forced harmonic motions of the airfoil in either plunging or pitching degree of freedom. In other words, only one degree of freedom is excited and the excitation of the other degree of freedom is fixed to zero. The specific mode of harmonic motions is determined by three variables, i.e., pitching amplitude $\alpha_{\max}$ or plunging amplitude $(h/b)_{\max}$, reduced frequency k and Mach number Ma. Besides, since the ROM is constructed in the time domain, the reduced frequency k is obtained from the number of time steps NT in each period as follows:

$$k = \frac{\omega b}{V} = \frac{\pi}{NT \cdot DT \cdot Ma} \tag{9}$$

The value of NT for test cases is set to 30, 60, 90, 120, 150, 180, 210 and 240. The range of reduced frequency is between 0.0260 and 0.2424, which is calculated from (9). The extrapolation capability of this proposed ROM is tested by using harmonic motions at Mach numbers 0.72 and 0.84.

Figures 10, 11, 12, 13 and 14 show hysteresis loops of typical test cases. In Figs. 10 and 11, a comparison of three test cases under different Mach numbers but the same pitching or plunging amplitude and NT between ROM and CFD simulations is given. Even though the difference in lift coefficient at different Mach numbers is relatively small, the proposed ROM can still identify this small deviation, as shown in Figs. 10a and 11a. However, the predictions of moment coefficient are less accurate than those of lift coefficient due to a stronger nonlinear effect.

Harmonic motions under different reduced frequencies but the same Mach number and amplitude are illus-

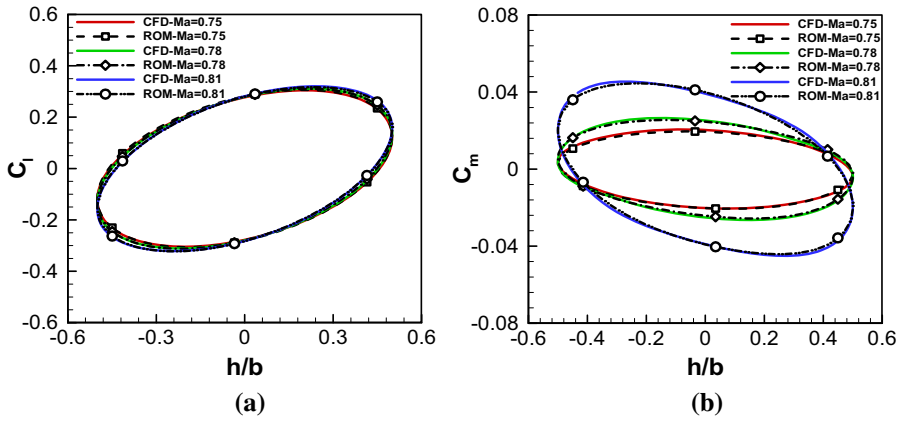

Fig. 11 Predictions of harmonic motions with plunging amplitude 0.5 and 90 steps in a period under different Mach numbers. **a** Lift coefficient. **b** Moment coefficients

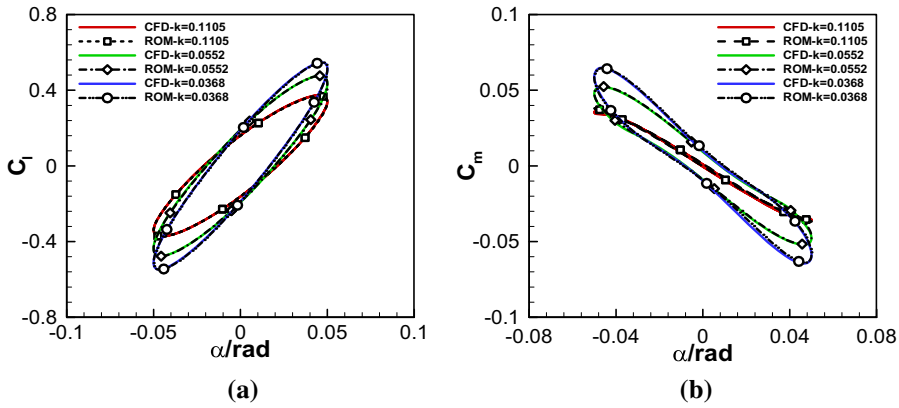

Fig. 12 Predictions of harmonic motions with pitching amplitude 0.05 and Mach number 0.79 under different reduced frequencies. **a** Lift coefficient. **b** Moment coefficients

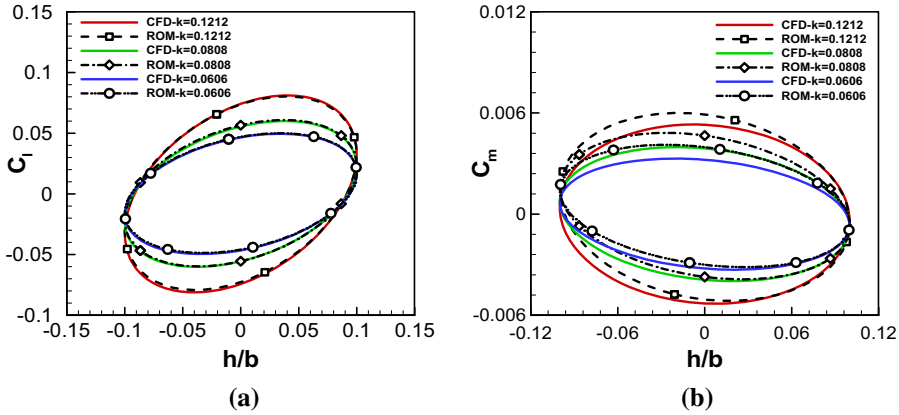

Fig. 13 Predictions of harmonic motions with pitching amplitude 0.1 and Mach number 0.72 (extrapolation) under different reduced frequencies. **a** Lift coefficient. **b** Moment coefficients

trated in Figs. 12, 13 and 14. It is obvious that the unsteady effects were characterized by reduced frequency from those two figures. As the reduced frequency k becomes larger, amplitude of lift and moment coefficient increases for pitching motions, but this trend reverses for plunging motions. When the flow is dominated by the linear dynamics, the shape of the hysteresis loop is elliptical. Therefore, the nonlinearity can be observed from the shape of the hysteresis loops. Aerodynamic nonlinearity arises at a large pitching amplitude, as illustrated in Fig. 12, where the amplitude 0.05 rad is shown. The nonlinear behavior is evident, especially for the moment. However, this ROM still can reflect the nonlinear aerodynamic precisely since the results predicted by this approach have good agreement with those obtained from CFD simulations. The extrap-

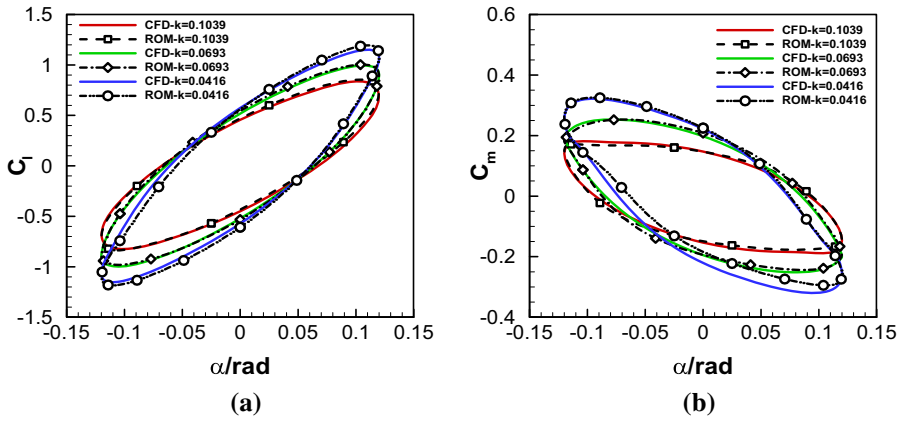

Fig. 14 Predictions of harmonic motions with plunging amplitude 0.12 and Mach number 0.84 (extrapolation) under different reduced frequencies. **a** Lift coefficient. **b** Moment coefficients

Table 1 Relative error comparison of all test cases

Degree of freedom	Ma	$(h/b)_{\max}$ or $\alpha_{\max}$	k	C_{l} (%)	C_{m} (%)
Plunging	0.75	0.09	0.0582	1.26	4.57
Plunging	0.78	0.09	0.0559	1.39	2.89
Plunging	0.81	0.09	0.0539	1.49	3.91
Pitching	0.75	0.5	0.0776	1.57	6.72
Pitching	0.78	0.5	0.0746	0.93	4.10
Pitching	0.81	0.5	0.0718	1.18	3.47
Plunging	0.79	0.05	0.1105	0.74	3.94
Plunging	0.79	0.05	0.0552	0.54	1.60
Plunging	0.79	0.05	0.0368	0.48	2.19
Pitching	0.72	0.1	0.1212	2.14	15.6
Pitching	0.72	0.1	0.0808	1.90	19.8
Pitching	0.72	0.1	0.0606	2.07	22.6
Plunging	0.84	0.12	0.1051	4.08	6.45
Plunging	0.84	0.12	0.0421	1.94	5.23
Plunging	0.84	0.12	0.0263	4.98	8.69

olation capability is examined in Figs. 13 and 14. As a data-driven model and a system identification method, it is obvious that no one method would be expected to perform well for all conceivable situations [13], even if a DNN model. The model performance relies largely on the training data. Therefore, we cannot expect the model to give satisfactory results for further analysis when the parameter of interest lies outside the range of parameters (e.g., Mach number, amplitude and frequency) it has been trained. However, those results from extrapolation can still be seen as a good reference in the dynamics beyond the parameter space.

Relative errors of all test cases in Figs. 10, 11, 12, 13 and 14 are reported in Table 1. The errors for lift and moment coefficient are within 2% and 7% for the modeling flight regime ($Ma = 0.74 \sim 0.82$), respectively. And the errors for lift coefficient are smaller than those for moment coefficient. Without any doubt, the biggest relative error is shown in extrapolated phase ($Ma = 0.72$ and 0.84) because of no information provided during model training for dynamics outside the parameter space. Moreover, the error at $Ma = 0.75$, plunging amplitude 0.5 and reduced frequency 0.0776 is relatively large because the model cannot get the information from this type of input data, where the performance of this ROM is not as good as other samples. In general, the overall ROM performance is achieved as expected for the most flow conditions.

For a further investigation on the ROM performance, the results of the ROM and CFD simulations

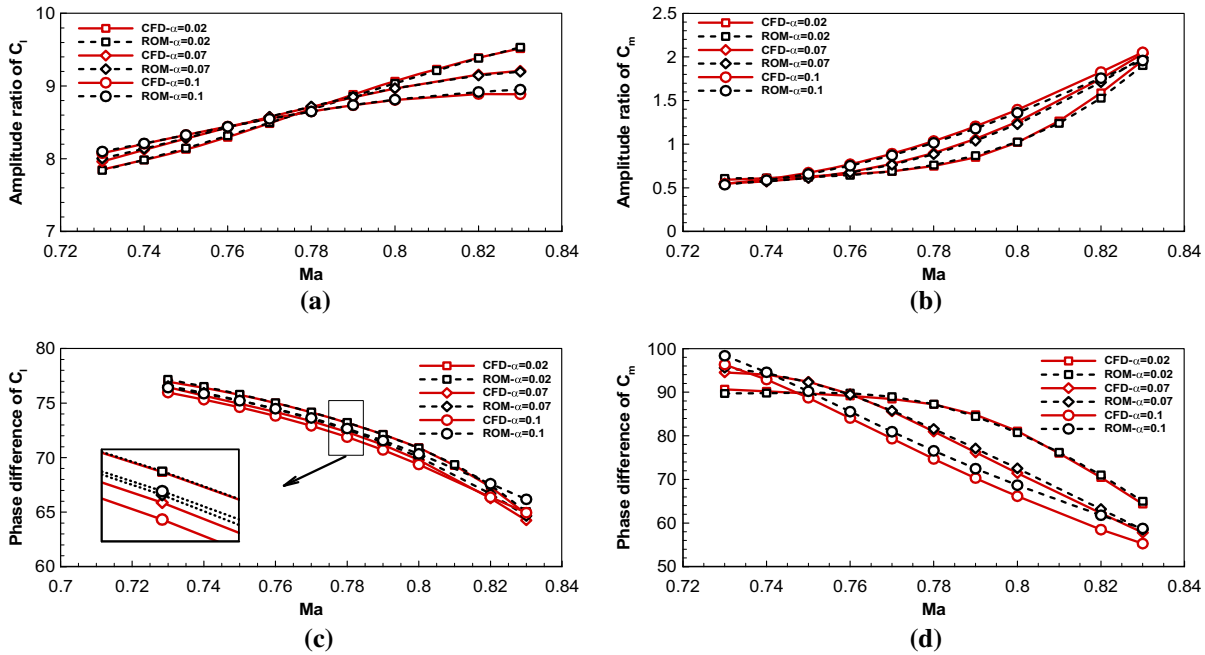

Fig. 15 First-order Fourier series of harmonic pitching motions with 120 steps in a period ($k = 0.0526 \sim 0.0598$). **a** Amplitude ratio of the lift coefficient. **b** Amplitude ratio of the moment coefficient. **c** Phase difference of the lift coefficient. **d** Phase difference of the moment coefficient

are compared in the frequency domain by using the fast Fourier transformation (FFT) method. The amplitude ratio (AR) and phase difference (PD) between the aerodynamic response and the structural motions are computed from FFT, and then the first-order components of amplitude and phase are used for comparison. Comparisons of AR and PD can reflect the capability of capturing the frequency characteristics for a model, which is very significant in analyzing the aeroelastic behaviors after coupling the aerodynamic model and the structural motion equations. In this study, there are two types of cases. The first one is harmonic pitching motion with $NT = 120$, whose Mach number changes from 0.73 to 0.83 ($k = 0.0526 \sim 0.0598$), and the influence of pitching amplitude is considered. As illustrated in Fig. 15, AR and PD change in an approximately linear fashion in the small pitching amplitude, but these parameters will change nonlinearly in the large pitching amplitude because of the aerodynamic nonlinearity induced by large motions of the shock wave. The relative error of CFD simulations and ROM is shown in Fig. 16, where the extrapolation error is relatively large. The second case includes harmonic pitching motions at Mach number 0.79, whose NT changes from 30 to 180 ($k = 0.0368 \sim 0.2209$). As seen in Fig. 17, AR and PD vary dramatically with reduced frequency k and pitching amplitude due to the strong shock wave at this flow condition, thus resulting in complex variations with different amplitudes and frequencies. Similarly, Fig. 18 shows the relative error of CFD simulations and ROM, which is still acceptable.

4.3 LCO trend and flutter characteristics

In this subsection, the aeroelastic system is studied by coupling the proposed ROM with the structural motion equations. In order to evaluate the ROM performance, the standard flow and structural parameters are used [57]. The structural parameters of a NACA64A010 airfoil are listed in the following:

$$\begin{aligned} a_0 &= 0^\circ \\ a &= -0.6 \\ x_a &= 0.25 \\ r_a^2 &= 0.75 \\ \omega_h/\omega_a &= 0.5 \\ \mu &= 75 \end{aligned} \tag{10}$$

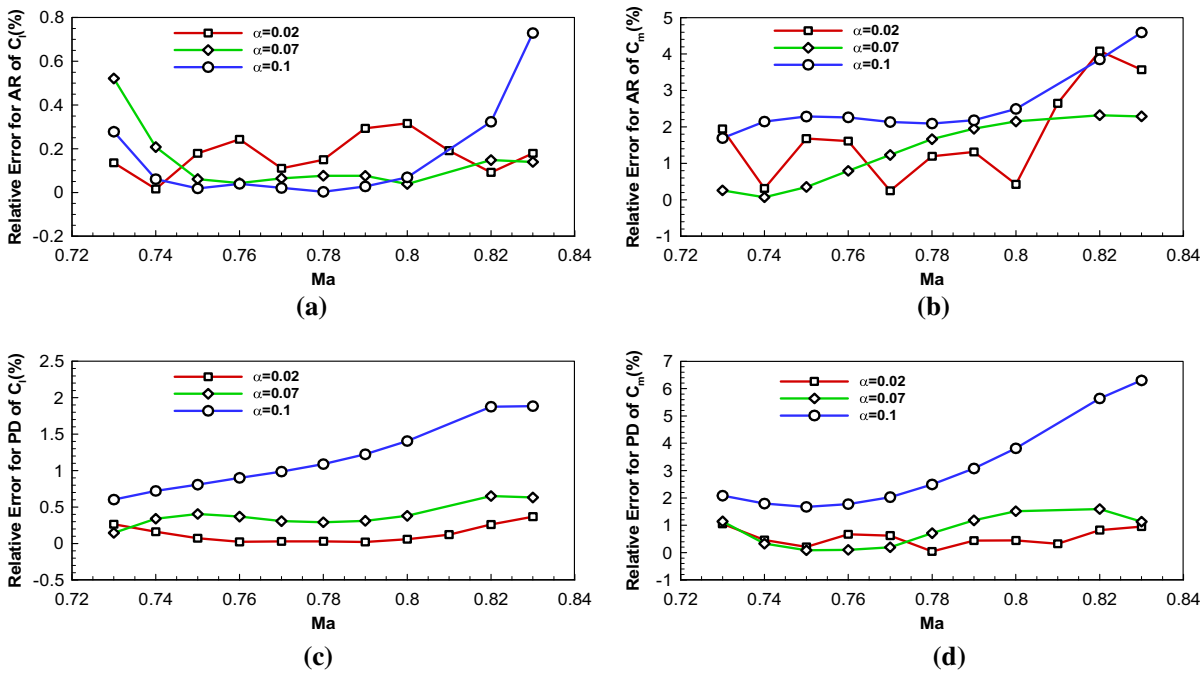

Fig. 16 Relative error of harmonic pitching motions with 120 steps in a period ($k = 0.0526 \sim 0.0598$). **a** Amplitude ratio of the lift coefficient. **b** Amplitude ratio of the moment coefficient. **c** Phase difference of the lift coefficient. **d** Phase difference of the moment coefficient

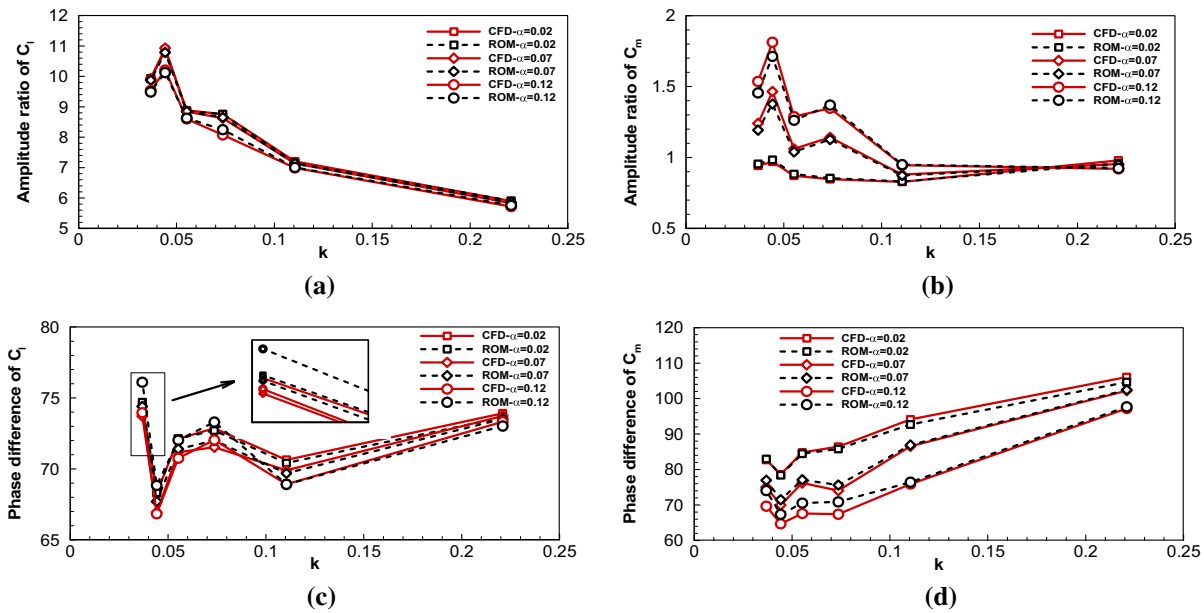

Fig. 17 First-order Fourier series of harmonic pitching motions at Mach number 0.79 ($k = 0.0276 \sim 0.2209$). **a** Amplitude ratio of the lift coefficient. **b** Amplitude ratio of the moment coefficient. **c** Phase difference of the lift coefficient. **d** Phase difference of the moment coefficient

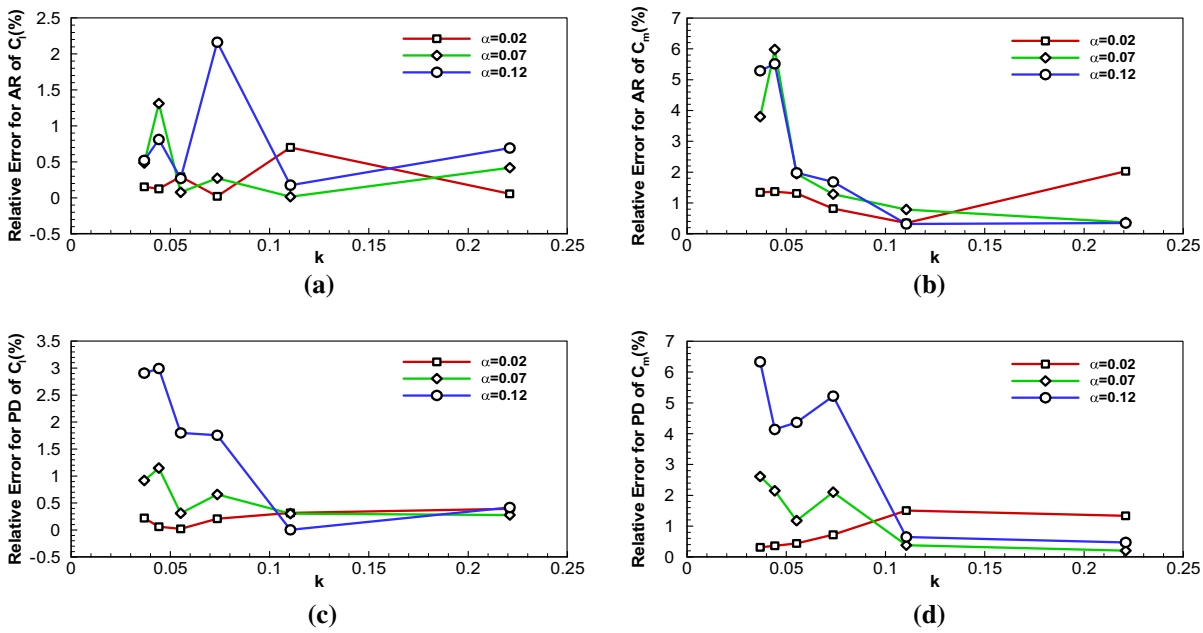

Fig. 18 Relative error of harmonic pitching motions at Mach number 0.79 ($k = 0.0276 \sim 0.2209$). **a** Amplitude ratio of the lift coefficient. **b** Amplitude ratio of the moment coefficient. **c** Phase difference of the lift coefficient. **d** Phase difference of the moment coefficient

As shown in Fig. 19, the LCO trends at Mach numbers 0.77, 0.78, 0.79, 0.80 and 0.81 are computed by both CFD simulations and ROM. Moreover, it is revealed that there is a good match between the two methods, but a relatively large error in some bifurcation points. Compared with the shallow neural network [26], the accuracy of this ROM has been greatly improved. Then, the LCO amplitude becomes larger as the Mach number decreases, which means that there exists a weaker aerodynamic nonlinearity. Thus, the linear dynamic behaviors can be reflected by this nonlinear ROM to a certain extent. It is worth highlighting that LCO trend is close to a straight line below Mach number 0.77 and the flutter-reduced velocity varies dramatically at Mach number 0.82. Therefore, only the LCO trends within Mach number 0.77 and 0.81 are given here.

Furthermore, the LCO trends with four changes of different structural parameters at standard Mach number 0.8 are considered. The frequency ratio ω_h/ω_α is set to 0.4 and 0.6, respectively, and the mass ratio μ is fixed to 40 and 200, respectively. It should be mentioned that for standard test case, $\mu = 75$ and $\omega_h/\omega_\alpha = 0.5$. All LCO trends are illustrated in Figs. 20 and 21, where the results of ROM have a good agreement with those of CFD simulations. Additionally, a higher mass ratio leads to a smaller bifurcation velocity and frequency, which is indicated by changes of reduced frequency due to the varying mass ratio, as seen in Fig. 20. Meanwhile, it is demonstrated that this model still has a good generalization ability for different structural parameters.

The LCO responses at $Ma = 0.78$, $V^* = 0.70$ and $Ma = 0.79$, $V^* = 0.72$ are depicted in Fig. 22, where the temporal responses from ROM and CFD simulations are consistent in amplitude and frequency. Multiple responses at the same reduced velocity and different Mach numbers are shown in Fig. 23. As seen in Fig. 23a, b, the velocity and displacement of pitching and plunging motions vary with reduced frequency k, respectively. The aeroelastic response is shown to be a LCO phenomenon and periodic motion. Hence, as illustrated in those figures, the proposed ROM can capture the velocity and displacement characteristics very well, even though the flow condition is varied.

4.4 Computational cost and comparison

In this subsection, the proposed model is compared with CFD simulation and a simple model called POD-

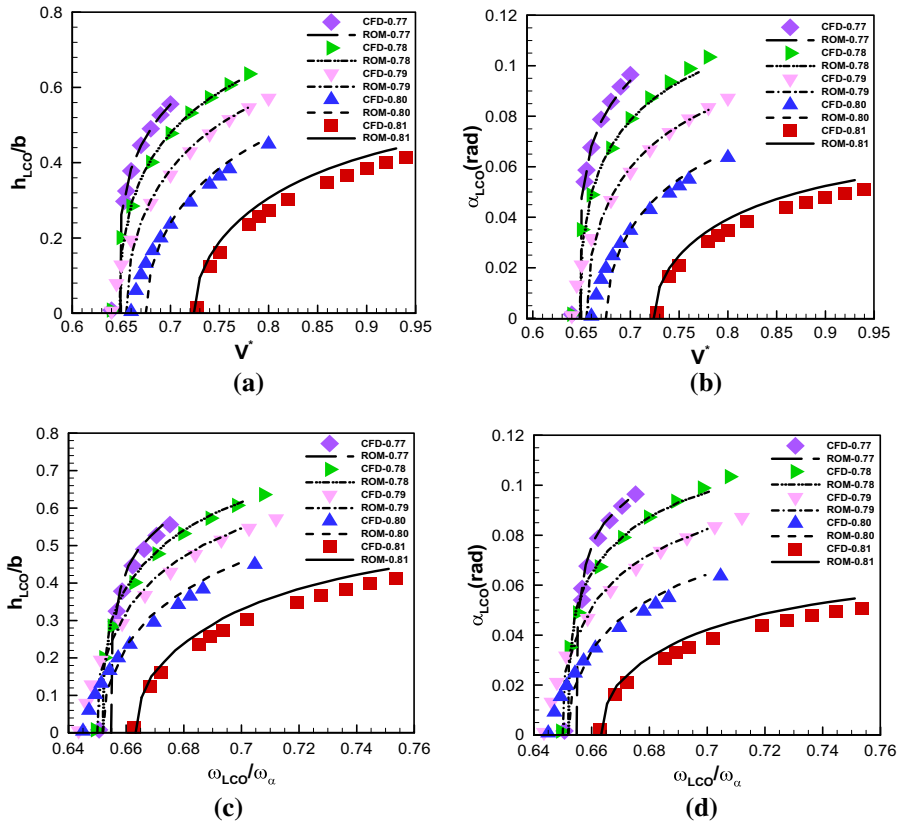

Fig. 19 Comparisons among LCO trends of a NACA64A010 airfoil. **a** Plunging amplitude versus LCO velocity. **b** Pitching amplitude versus LCO velocity. **c** Plunging amplitude versus LCO frequency. **d** Pitching amplitude versus LCO frequency

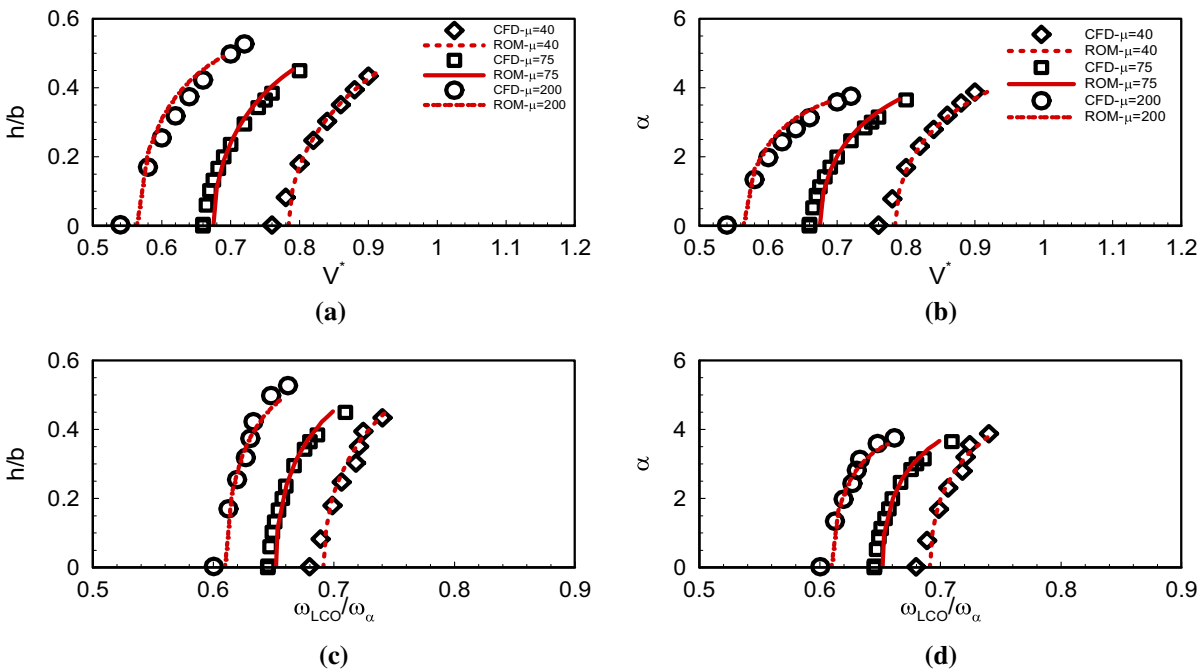

Fig. 20 LCO trends with different mass ratios. **a** Plunging amplitude versus LCO velocity. **b** Pitching amplitude versus LCO velocity. **c** Plunging amplitude versus LCO frequency. **d** Pitching amplitude versus LCO frequency

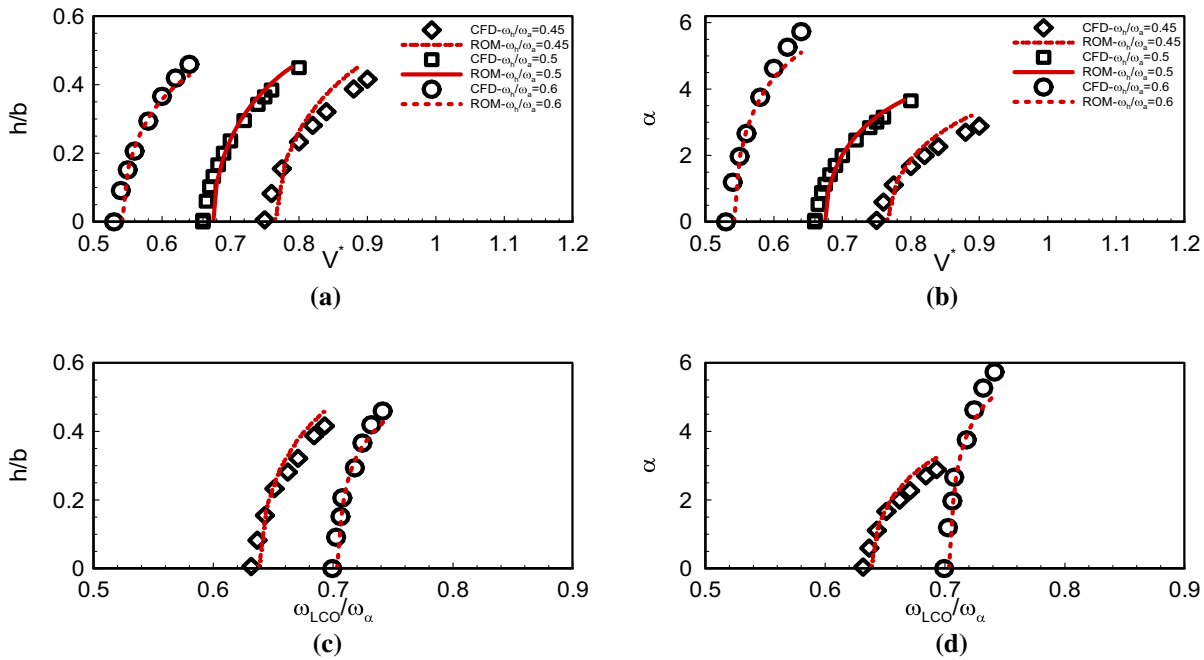

Fig. 21 LCO trends with different frequency ratios. **a** Plunging amplitude versus LCO velocity. **b** Pitching amplitude versus LCO velocity. **c** Plunging amplitude versus LCO frequency. **d** Pitching amplitude versus LCO frequency

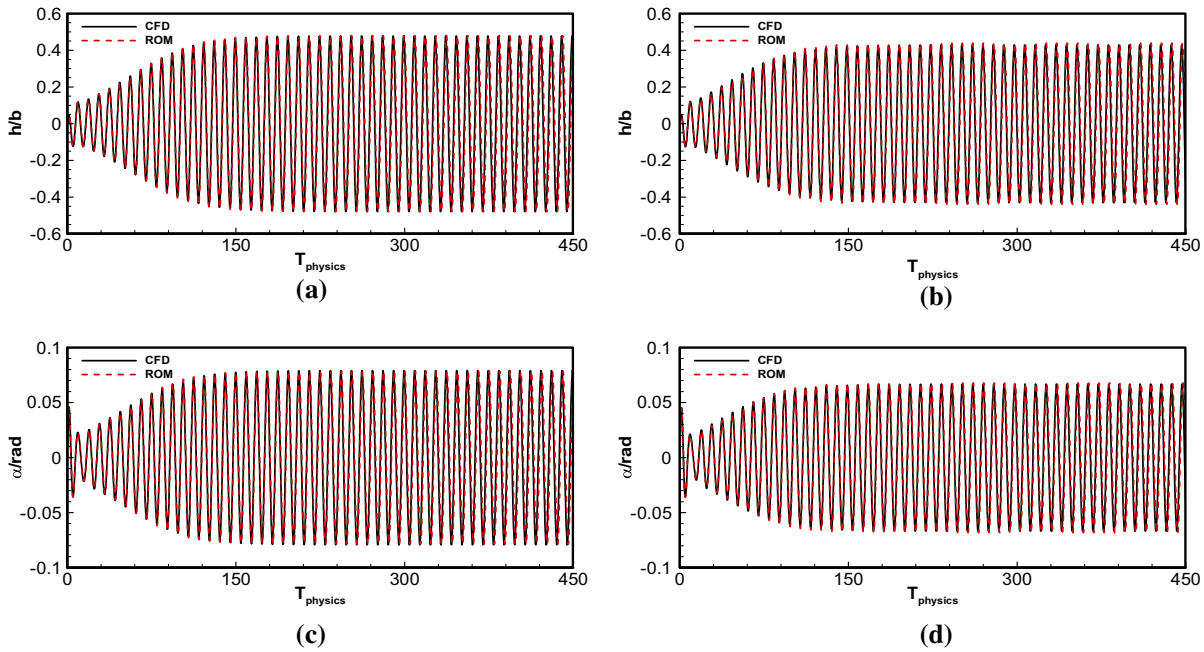

Fig. 22 LCO responses. **a** $Ma = 0.78$, $V^* = 0.70$, plunging motion versus time. **b** $Ma = 0.79$, $V^* = 0.72$, plunging motion versus time. **c** $Ma = 0.78$, $V^* = 0.70$, pitching motion versus time. **d** $Ma = 0.79$, $V^* = 0.72$, pitching motion versus time

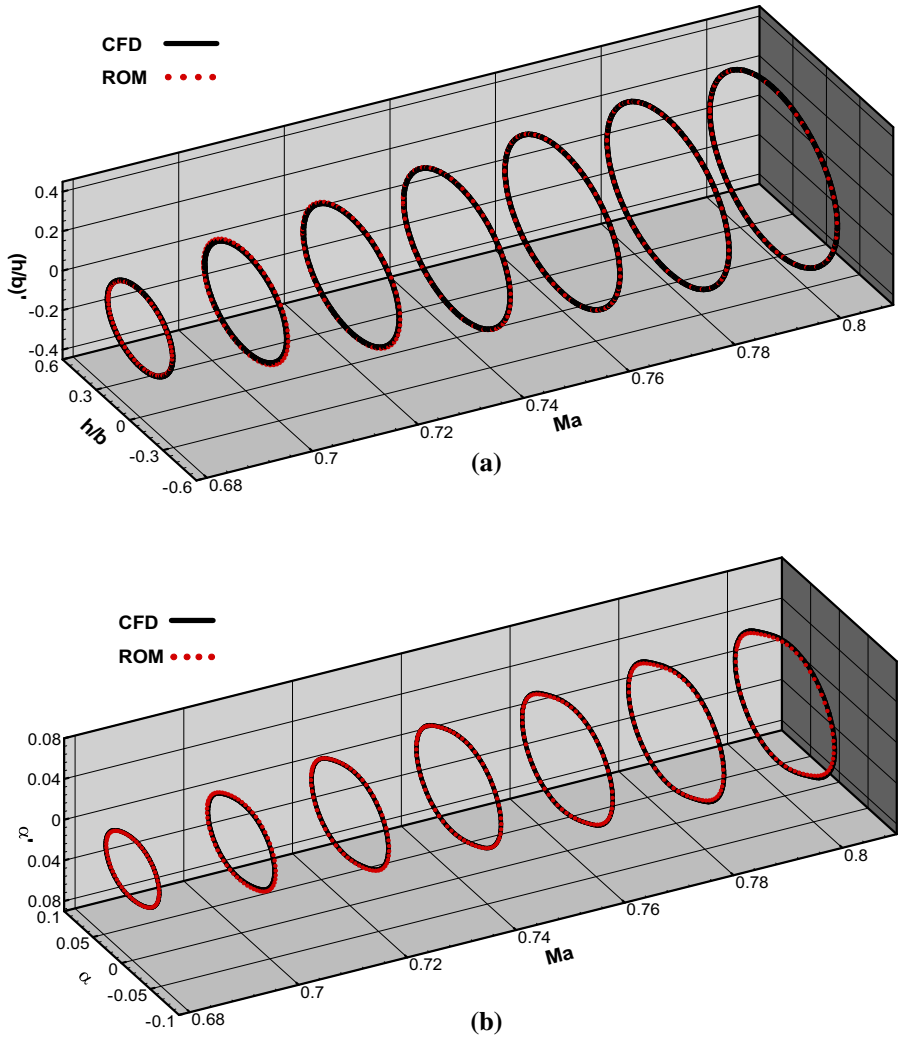

Fig. 23 Velocity and displacement versus reduced frequency k. **a** Plunging motions. **b** Pitching motions

RBF network, which is developed by Zhang et al. [26,28]. The comparison of aeroelastic simulation and time cost is shown in Fig. 24 and Table 2. In these figures, POD-RBF-simpler refers to the ROM based on POD-RBF network for a single Mach number [28], while POD-RBF refers to the ROM based on POD-RBF network for multiple Mach numbers (the training cases are the same as those of the current study) [26]. ROM still refers to the proposed aerodynamic model based on LSTM network.

The development of ROM is mainly due to the high computational cost of aerodynamic simulation. As reported in Table 3, the computational burden for CFD simulations is extremely huge, and a total computation time of 605 h is needed for all test cases. For the aerodynamic ROMs, calculating the training data is the main source of the computational cost. Each set of training and validation cases contains 3500 and 1000 time steps, respectively, which consumes about 32 h for the proposed ROM and 24 h for POD-RBF (this model does not require the validation case because the model is difficult to fit the training data [26]). The ROM and POD-RBF training needs about 6 h and 2 h due to the optimization of parameters, respectively. A different NT results in varying time for different harmonic motions. Since the average time steps in a period are nearly 130, each harmonic motion by CFD, ROM and POD-RBF is approximately estimated as 1 h, 0.1 s and 5 s, respectively. In different computational conditions, time for calculating stable LCO responses is different. Consequently, it is a rough estimation that the computational time for each LCO response by CFD, ROM and

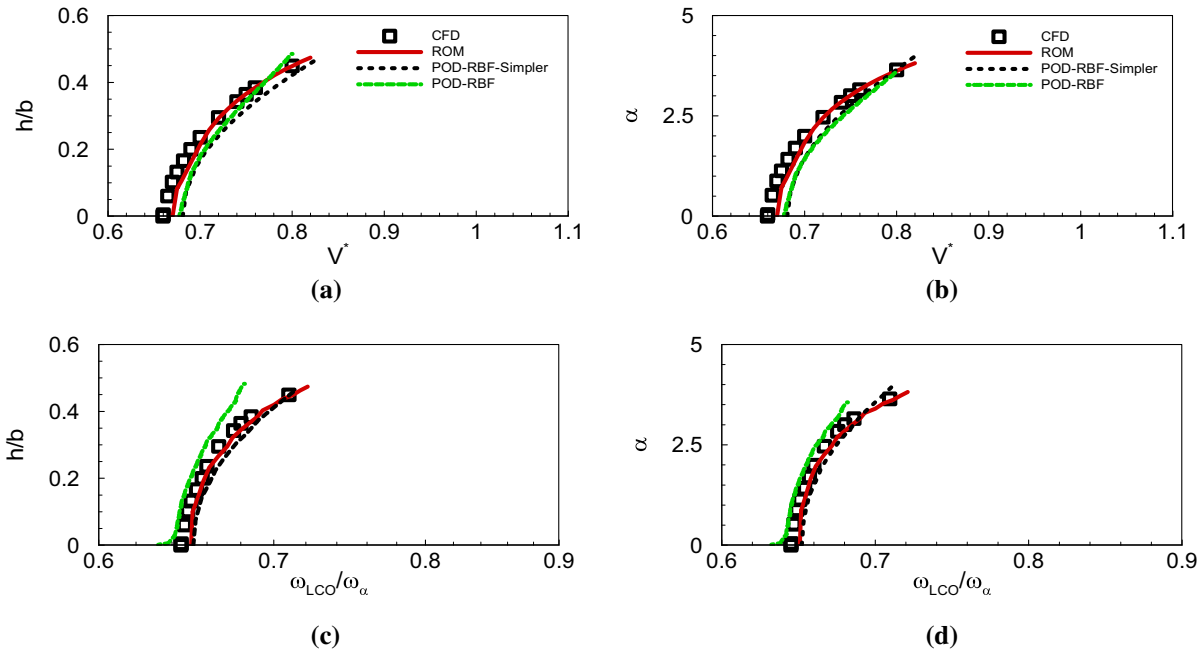

Fig. 24 LCO trends at $Ma = 0.8$, $\alpha_0 = 0\,\text{deg}$, $a = -0.6$, $x_\alpha = 0.25$, $r_\alpha^2 = 0.75$, $\omega_h/\omega_\alpha = 0.5$ and $\mu = 75$. **a** Plunging amplitude versus LCO velocity. **b** Pitching amplitude versus LCO velocity. **c** Plunging amplitude versus LCO frequency. **d** Pitching amplitude versus LCO frequency

Table 2 Relative error comparison between LSTM network and POD-RBF

Degree of freedom	Ma	$\alpha_{\max}$ or $(h/b)_{\max}$	k	C_l (%) POD-RBF/ROM	C_m (%) POD-RBF/ROM
Pitching	0.75	0.07	0.0582	2.91/0.91	14.58/3.48
Pitching	0.79	0.07	0.0552	2.99/1.41	4.87/4.45
Pitching	0.82	0.07	0.0532	5.25/1.90	8.79/4.79
Plunging	0.74	0.3	0.0472	7.31/1.41	10.35/3.75
Plunging	0.78	0.3	0.0448	5.34/0.83	17.68/3.77
Plunging	0.81	0.3	0.0431	7.22/1.47	9.10/2.31
Pitching	0.79	0.09	0.1105	4.13/0.87	11.62/6.52
Pitching	0.79	0.09	0.0736	5.67/1.72	8.85/3.76
Pitching	0.79	0.09	0.0442	2.88/1.88	7.45/4.53
Plunging	0.73	0.5	0.1195	5.20/1.15	19.01/7.47
Plunging	0.73	0.5	0.0598	5.59/1.74	13.16/3.86
Plunging	0.73	0.5	0.0398	8.49/1.65	18.54/6.58

POD-RBF is 6 h, 60 s and 20 s respectively. It is obvious that the proposed approach achieves higher modeling accuracy at the cost of a fraction of computation. However, it is acceptable and with the increasing samples or in a more complicated system, the computational efficiency can be improved dramatically. Besides, the computation time of ROM is reduced by about one order of magnitude compared with that of CFD.

Table 3 Comparison between the time cost of CFD and ROM

Method	Time cost	Total time
CFD Simulations	(1) Time cost for each harmonic motion is about 1 h; Time cost for each LCO response is about 6 h	$(1\times203)\,\mathrm{h}+6\times(52+15)\mathrm{h} = 605\,\mathrm{h}$
	(2) There are 203 harmonic motions, 52 LCO responses for standard condition, 15 cases for the variations of structural parameters	
ROM	(1) Time cost for ROM training is about 6 h	$6\,\mathrm{h} + 203 \times 0.1\,\mathrm{s} + (52 + 15) \times 60\,\mathrm{s} + 32\,\mathrm{h} = 39.12\,\mathrm{h}$
	(2) Each harmonic motion and LCO response cost 0.1 s and 60 s, respectively	
	(3) Time cost for CFD simulations of training and validation case is about 32 h	
POD-RBF	(1) Time cost for ROM training is about 2 h	$2\,\mathrm{h} + 203 \times 5\,\mathrm{s} + (52 + 15) \times 20\,\mathrm{s} + 24\,\mathrm{h} = 26.65\,\mathrm{h}$
	(2) Each harmonic motion and LCO response cost 5 s and 20 s, respectively	
	(3) Time cost for CFD simulations of training and validation case is about 24 h	

5 Conclusions

In this paper, an unsteady aerodynamic ROM across multiple Mach numbers based on deep learning method is presented. Deep learning is very good at discovering hidden information and intricate structures in large amount of high-dimensional data and requires very little engineering by hand. A typical deep neural network, the long short-term memory network (LSTM) network, is used to predict the aerodynamic loads and aeroelastic responses under different Mach numbers. A transonic NACA 64A010 airfoil with two degrees of freedom is studied in this work. From test cases, four main conclusions are drawn:

(1) The linear and nonlinear aerodynamic characteristics at different amplitudes and frequencies under different Mach number can be captured precisely by the proposed ROM.
(2) This ROM can accurately capture the LCO characteristics and flutter boundary of aeroelastic system under different Mach numbers and structural parameters.
(3) The computational efficiency of this ROM is enhanced by at least one order of magnitude compared with that of CFD simulations. Specifically, in the current study, the time cost of ROM is only 6% of CFD computation. And the ROM achieves higher modeling accuracy than simpler models at the cost of a fraction of computation.
(4) The unsteady, nonlinear aerodynamic model based on deep neural networks can improve the generalization capability of traditional aerodynamic ROMs dramatically and shows high accuracy in predicting aerodynamic characteristics under different flow conditions.

In general, it is demonstrated in this work that deep learning is well suited in the study of unsteady aerodynamics and has great potential in developing an aerodynamic model with higher generalization capability and better robustness to operating conditions. In the future, the proposed deep learning-based aerodynamic model will be applied to many complicated aerodynamic and aeroelastic problems with multiple degrees of freedom, e.g., three-dimensional aircraft, aeroservoelasticity, model order reduction of unsteady flowfield and so on.

Acknowledgements This work was supported by the National Natural Science Foundation of China (No. 11572252), the National Science Fund for Excellent Young Scholars (No. 11622220) and "111" project of China (No. B17037) and ATCFD project (2015-F-016). We thank Professor Bernd Noack of LIMSI-CNRS for his valuable discussions and suggestions on this work.

Compliance with ethical standards

Conflict of interest The authors declare that there is no conflict of interest in preparing this article.

References

1. Chen, G., Sun, J., Li, Y.: Active flutter suppression control law design method based on balanced proper orthogonal decomposition reduced order model. Nonlinear Dyn. **70**, 1–12 (2012)
2. Da Ronch, A., Badcock, K.J., Wang, Y., Wynn, A., Palacios, R.: Nonlinear model reduction for flexible aircraft control design. In: AIAA Atmospheric Flight Mechanic Conference, AIAA- 2012-4404. American Institute of Aeronautics and Astronautics, Minneapolis, Minnesota (2012)
3. Brunton, S., Noack, B.: Closed-loop turbulence control: progress and challenges. Appl. Mech. Rev. **67**(5), 050801 (2015)
4. Wang, Z., Zhang, W., Wu, X., Chen, K.: A novel unsteady aerodynamic reduced-order modeling method for transonic aeroelastic optimization. J. Fluid. Struct. **82**, 308–328 (2018)
5. Zhang, W., Li, X., Ye, Z., Jiang, Y.: Mechanism of frequency lock-in in vortex-induced vibrations at low Reynolds numbers. J. Fluid Mech. **783**, 72–102 (2015)
6. Gao, C., Zhang, W., Li, X., Liu, Y., Quan, J., Ye, Z., Jiang, Y.: Mechanism of frequency lock-in in transonic buffeting flow. J. Fluid Mech. **818**, 528–561 (2017)
7. Hesse, H., Palacios, R.: Reduced-order aeroelastic models of maneuvering flexible aircraft. AIAA J. **52**(8), 1717–1732 (2014)
8. Lucia, D.J., Beran, P.S., Silva, W.A.: Reduced-order modeling: new approaches for computational physics. Prog. Aerosp. Sci. **40**(1–2), 51–117 (2004)
9. Ghoreyshi, M., Jirasek, A., Cummings, R.M.: Reduced order unsteady aerodynamic modeling for stability and control analysis using computational fluid dynamics. Prog. Aerosp. Sci. **71**, 167–217 (2014)
10. Kou, J., Zhang, W.: A hybrid reduced-order framework for complex aeroelastic simulations. Aerosp. Sci. Technol. **84**, 880–894 (2019)
11. Willcox, K., Peraire, J.: Balanced model reduction via the proper orthogonal decomposition. AIAA J. **40**(11), 2323–2330 (2002)
12. Schmid, P.J.: Dynamic mode decomposition of numerical and experimental data. J. Fluid Mech. **656**, 5–28 (2010)
13. Brewick, P.T., Masri, S.F.: An evaluation of data-driven identification strategies for complex nonlinear dynamic systems. Nonlinear Dyn. **85**, 1297–1318 (2016)
14. He, S., Yang, Z., Gu, Y.: Nonlinear dynamics of an aeroelastic airfoil with free-play in transonic flow. Nonlinear Dyn. **87**, 2099–2125 (2017)
15. Zhang, W., Ye, Z.: Reduced-order-model-based flutter analysis at high angle of attack. J. Aircr. **44**(6), 2086–2089 (2007)
16. Zhang, W., Wang, B., Ye, Z., Quan, J.: Efficient method for limit cycle flutter analysis based on nonlinear aerodynamic reduced-order models. AIAA J. **50**(5), 1019–1028 (2012)
17. Da Ronch, A., Ghoreyshi, M., Badcock, K.J.: On the generation of flight dynamics aerodynamic tables by computational fluid dynamics. Prog. Aerosp. Sci. **47**(8), 597–620 (2011)
18. Kou, J., Zhang, W., Yin, M.: Novel Wiener models with a time-delayed nonlinear block and their identification. Nonlinear Dyn. **85**, 2389–2404 (2016)
19. Duriez, Thomas, Brunton, Steven L., Noack, Bernd R.: Machine Learning Control-Taming Nonlinear Dynamics and Turbulence. Springer, Switzerland (2017)
20. Tracey, B.D., Duraisamy, K., Alonso, J.J.: A machine learning strategy to assist turbulence model development. In: 53rd AIAA Aerospace Sciences Meeting, AIAA SciTech, Kissimmee, FL (2015)
21. Mannarino, A., Mantegazza, P.: Nonlinear aeroelastic reduced order modeling by recurrent neural networks. J. Fluid. Struct. **48**, 103–121 (2014)
22. Amsallem, D., Farhat, C.: Interpolation method for adapting reduced-order models and application to aeroelasticity. AIAA J. **46**(7), 1803–1813 (2008)
23. Skujins, T., Cesnik, C.E.S.: Reduced-order modeling of unsteady aerodynamics across multiple mach regimes. J. Aircr. **51**(6), 1681–1704 (2014)
24. Winter, M., Breitsamter, C.: Neurofuzzy-model-based unsteady aerodynamic computations across varying freestream conditions. AIAA J. **54**(9), 2705–2720 (2016)
25. Liu, H., Huang, R., Zhao, Y., Hu, H.: Reduced-order modeling of unsteady aerodynamics for an elastic wing with control surfaces. J. Aerosp. Eng. **30**(3), 04016083 (2016)
26. Kou, J., Zhang, W.: Reduced-order modeling for nonlinear aeroelasticity with varying Mach numbers. J. Aerosp. Eng. **31**(6), 04018105 (2018)
27. Liu, H., Hu, H., Zhao, Y., et al.: Efficient reduced-order modeling of unsteady aerodynamics robust to flight parameter variations. J. Fluids Struct. **49**(8), 728–741 (2014)
28. Zhang, W., Kou, J., Wang, Z.: Nonlinear aerodynamic reduced-order model for limit-cycle oscillation and flutter. AIAA J. **54**(10), 3302–3310 (2016)
29. Schmidhuber, J.: Deep learning in neural networks: an overview. Neural Netw. **61**, 85–117 (2015)
30. Sainath, T.N., Mohamed, A.R., Kingsbury, B., Ramabhadran, B.: Deep convolutional neural networks for LVCSR. In: 2013 IEEE International Conference on Acoustics, Speech and Signal Processing (ICASSP), pp. 8614–8618 (2013)
31. Krizhevsky, A., Sutskever, I., Hinton, G.E.: Imagenet classification with deep convolutional neural networks. In: 2012 International Conference on Neural Information Processing Systems, pp. 1097–1105 (2012)
32. Xiong, H., Alipanahi, B., et al.: The human splicing code reveals new insights into the genetic determinants of disease. Science **347**(6218), 1254806 (2015)
33. Jin, X., Shao, J., Zhang, X., An, W., Malekian, R.: Modeling of nonlinear system based on deep learning framework. Nonlinear Dyn. **84**, 1327–1340 (2016)
34. Rosa, E.D.L., Yu, W.: Randomized algorithms for nonlinear system identification with deep learning modification. Inf. Sci. **364–365**, 197–212 (2016)
35. Ling, J., Kurzawski, A., Templeton, J.: Reynolds averaged turbulence modeling using deep learning neural networks with embedded invariance. J. Fluid Mech. **807**, 155–166 (2016)
36. Efrati, A.: Apples machines can learn too. The Information. https://www.theinformation.com/articles/apples-machines-can-learn-too (2016). Accessed 13 June 2016
37. Vogels, W.: Bringing the magic of amazon ai and alexa to apps on aws. All Things Distributed. https://www.allthingsdistributed.com (2016). Accessed 30 Nov 2016

38. Zhao, Z., Chen, W., Wu, X., et al.: LSTM network: a deep learning approach for short-term traffic forecast. IET Intell. Transp. Syst. **11**(2), 68–75 (2017)
39. Fu, R., Zhang, Z., Li L.: Using LSTM and GRU neural network methods for traffic flow prediction. In: 2016 31st Youth Academic Annual Conference of Chinese Association Automation, pp. 324–328 (2016)
40. Wang, Z., Xiao, D., Fang, F., Govindan, R., Pain, C.C., Guo, Y.: Model identification of reduced order fluid dynamics systems using deep learning. Int. J. Numer. Meth. Fluids. **86**(4), 255–268 (2018)
41. Mohan, A.T., Gaitonde, D.V.: A Deep Learning based Approach to Reduced Order Modeling for Turbulent Flow Control using LSTM Neural Networks (2018). arXiv:1804.09269v1 [physics.comp-ph]
42. LeCun, Y., Bengio, Y., Hinton, G.E.: Deep learning. Nature **521**(7553), 436–444 (2015)
43. Hochreiter, S., Schmidhuber, J.: Long short-term memory. Neural Comput. **9**(8), 1735–1780 (1997)
44. Pascanu. R., Mikolov, T., Bengio, Y.: On the difficulty of training recurrent neural networks. In: International Conference on International Conference on Machine Learning. JMLR.org, III-1310 (2013)
45. Chollet, F.: Keras (2015). https://github.com/fchollet/keras
46. Kou, J., Zhang, W.: Multi-kernel neural networks for nonlinear unsteady aerodynamic reduced-order modeling. Aerosp. Sci. Technol. **67**, 309–326 (2017)
47. Kou, J., Zhang, W.: An approach to enhance the generalization capability of nonlinear aerodynamic reduced-order models. Aerosp. Sci. Technol. **49**(1), 197–208 (2016)
48. Goodfellow, Ian, Bengio, Yoshua, Courville, Aaron: Deep Learning, pp. 246–252. MIT Press, Cambridge (2016)
49. Jiang, Y.: Numerical Solution of Navier–Stokes Equations on Generalized Mesh and Its Applications. Ph.D. Dissertation, Northwestern Polytechnical Univ., Xi'an, China (2013)
50. Boer, A., Schoot, M.S., Faculty, H.B.: Mesh deformation based on radial basis function interpolation. Comput. Struct. **85**(11–14), 784–795 (2007)
51. Zhang, W., Gao, C., Liu, Y., Ye, Z., Jiang, Y.: The interaction between flutter and buffet in transonic flows. Nonlinear Dyn. **82**(4), 1851–1865 (2015)
52. Gao, C., Zhang, W., Liu, Y., Ye, Z., Jiang, Y.: Numerical study on the correlation of transonic single-degree-of-freedom flutter and buffet. Sci. China Phys. Mech. Astron. **58**(8), 084701 (2015)
53. Zhang, W., Jiang, Y., Ye, Z.: Two better loosely coupled solution algorithms of CFD based aeroelastic simulation. Eng. Appl. Comput. Fluid Mech. **1**(4), 253–262 (2007)
54. Graves, A., Mohamed, A.R., Hinton G.E.: Speech recognition with deep recurrent neural networks. In: 2013 IEEE International Conference on Acoustics, Speech and Signal Processing (ICASSP), pp. 6645–6649 (2013)
55. Pascanu, R., Gulcehre, C., Cho, K., Bengio, Y.: How to construct deep recurrent neural networks (2013). arXiv:1312.6026 [cs.NE]
56. Kingma, D., Adam B.J.: A method for stochastic optimization (2014). arXiv:1412.6980 [cs.LG]
57. Thomas, J.P., Dowell, E.H., Hall, K.C.: Nonlinear inviscid aerodynamic effects on transonic divergence, flutter and limit cycle oscillations. AIAA J. **40**(4), 638–646 (2002)